Nanoscale

PAPER

View Article Online
View Journal | View Issue

Cite this: *Nanoscale*, 2024, **16**, 19254

Design of multi-responsive and actuating microgels toward on-demand drug release†

Priyanshi Agnihotri, ‡[a] Divya Dheer,‡[a,b] Anvi Sangwan,[c] Vysakh C. Chandran,[a] Nimisha A. Mavlankar,[a] Gunjan Hooda,[a] Debabrata Patra *[c] and Asish Pal *[a]

Multifunctional colloidal microgels that exhibit stimuli-responsive behaviour and excellent biocompatibility have attracted particular attention for developing functional compartmentalized networks. Herein, a series of stimuli-responsive microgels (**M0**, **M1**, and **M2**) were designed through the copolymerization of di(ethylene glycol) methyl ether methacrylate (DEGMA) and methacrylic acid (MAA) monomers using hydroxy ethyl methacrylate-coupled azobenzene (HEMA-Az) and ethylene glycol dimetharylate (EGDMA) as crosslinkers. The behaviour of the microgels in response to temperature, pH, and light was thoroughly investigated using spectroscopic, microscopic, and light-scattering techniques. Interestingly, the microgels deswelled with an increase in temperature, decrease in pH, and under the irradiation of UV light. Such a reversible swelling/deswelling behaviour was exploited for microgel **M2**, which showed better photoactuation at pH 5 with a higher fluid pumping velocity. The actuating microgel **M2** was optimized for loading the drug ciprofloxacin (**Cf**) to study its release at different temperature, pH, and light conditions. Microgel **M2** exhibited photoresponsive **Cf** release at pH 5 and 37 °C, demonstrating its potential for application in on-demand drug release.

Received 1st July 2024,
Accepted 6th September 2024

DOI: 10.1039/d4nr02728k

rsc.li/nanoscale

Introduction

The fascinating complexity of living cells in terms of their hierarchical molecular organization and adaptability to different environmental triggers has motivated the scientific community towards developing artificial cells as compartmentalized synthetic networks.[1–4] Bottom-up strategies, such as conversion of nanogels into microgels *via* precipitation polymerization and conversion of microgels into coacervates *via* emulsion polymerization/ligation/Janus-like phase separation, have recently been adopted for higher order compartmentalization in colloids.[5–7] In this regard, a number of physicochemical parameters, *e.g.* hydrophobicity, charge density, molecular flexibility, degree of crosslinking, stratify the hierarchical ordering in these synthetic compartments as oligomers, coacervates, microgels, hydrogels, fibres, *etc*.[8,9] Microgels consist of a spherical 3D-crosslinked network with a size ranging from 10 nm to a few microns with appreciable colloidal stability and possess a porous structure with a high surface area to volume ratio.[10] Recently, emergent functional synthetic systems, such as self-dividing and growing coacervates, stimuli-responsive and catalytically active coacervates, and nano/microcontainers for cargo storage and delivery, have attracted interest with regards to their compartmentalization, adaptivity, and structural integrity.[11–14] The incorporation of stimuli-responsive moieties in microgels renders a variable response to the local environment *e.g.* temperature, pH, light, solvent, ionic strength, electric or magnetic field, which is reflected in the reversible swelling/deswelling behaviour.[15–20] Moreover, polymeric microgels can be loaded with functional monomers and a variety of cargoes, such as enzymes and drugs, to exhibit on-demand on-site release and delivery applications. This spatio-temporal control over drug release reduces the risk of a sub-therapeutic dose of the drug in the target area.[21–29] Snowden *et al.* was the first to report the use of the PNIPAM microgel as a carrier to release acetylsalicylic acid and fluorescein-labelled dextran owing to PNIPAM's thermo-responsive characteristic at physiological temperature.[30,31] Recently, oligo(ethylene glycol) methacrylate (OEGMA)-based polymers have attracted great interest owing to their NIPAM-like thermo-responsiveness, polyethylene glycol (PEG)-like excellent biocompatibility and biodegradability.[32] Lu *et al.* reported OEGMA-based

[a]*Chemical Biology Unit, Institute of Nano Science and Technology, Knowledge City, Sector 81, Mohali 140306, Punjab, India. E-mail: apal@inst.ac.in*
[b]*Chitkara University School of Pharmacy, Chitkara University, Baddi 174103, Himachal Pradesh, India*
[c]*Energy and Environment Unit, Institute of Nano Science and Technology, Knowledge City, Sector 81, Mohali 140306, Punjab, India. E-mail: patra@inst.ac.in*
†Electronic supplementary information (ESI) available. See DOI: https://doi.org/10.1039/d4nr02728k
‡These authors contributed equally.

triply-responsive microgels using coumarin methacrylate to demonstrate the light-triggered release of the drug doxorubicin.[33]

Our group has also explored coumarin, ferrocene-tethered polymer chain collapse in segmented block co-polymeric systems towards tailored self-healing, catalysis, drug release, and ECM design.[34–41] Azobenzene with its outstanding reversible photoisomerization properties and offering the ability to precisely modulate its isomerization wavelength through minor structural modifications is an ideal candidate for use as a photoswitch in various applications. Further, we exploited a photoresponsive azobenzene motif with an excellent photoswitching ability between its *cis* and *trans* states for on-demand peptide piezoelectronics[42,43] and self-propelling or fluid pump devices owing to its conformation-induced mass-transfer capabilities.[44,45] Moreover, light-driven drug activation and release as mediated by azobenzene has recently emerged as an active area of photopharmacology.[46,47] Interestingly, advancements in these fields have now started to focus on self-propelling or fluid-actuation-based drug-delivery systems to access low permeability or physiologically unfavourable disease sites to overcome the limitations of passive drug release.[48] Therefore, we hypothesized that it would be possible to control the outward flow motion of a fluid (fluid flow) based on the swelling/deswelling of microgels *via* the photoactuation of azobenzene, which could then be used in an on-demand drug-release system, which would therefore not solely rely on pH and temperature cues.

Herein, we designed multi-responsive (temperature, pH, and light) microgels *via* the copolymerization of OEGMA, methacrylic acid (MAA) monomers along with ethylene glycol dimethacrylate (EGDMA) and photoresponsive azobenzene-tethered hydroxy ethyl methacrylate (HEMA-Az) crosslinkers (Scheme 1). The characterization and stimuli-responsive behaviour of the microgels were studied extensively using microscopy, spectroscopy, and scattering techniques. Interestingly, the microgels exhibited photoactuation multiple times, which was further explored towards exploiting the fluid flow pattern with both inward and outward flow for the first time. Further, we demonstrated the efficient loading of ciprofloxacin in the microgels and its on-demand release under orthogonal and combined stimuli triggers as a proof-of-concept for drug release propelled by fluid flow for the first time. Such photoresponsive microgels could potentially allow designing and developing photoactuating fluid micropumps that are adaptable to the external environment and capable of selectively delivering a drug to the active site.

Experimental section

Materials

Di(ethylene glycol) methyl ether methacrylate (DEGMA), methacrylic acid (MAA), ethylene glycol dimethacrylate (EGDMA), and ciprofloxacin hydrochloride monohydrate were obtained from Tokyo Chemical Industry. Potassium peroxodisulfate (KPS, 99%) was purchased from Merck, Germany. All the chemicals were of analytical grade and used as received. Milli-Q water with a resistivity of 18.2 MΩ cm at 25 °C was used to prepare all the solutions.

Synthesis of the microgels

Synthesis of the microgels was carried out *via* free radical precipitation polymerization.[49,50] Three microgels (**M0**, **M1**, **M**) were prepared by tuning the crosslinker concentration according to the reactions compositions in Table 1 and according to the following preparation process. The appropriate amounts of di(ethylene glycol) methyl ether methacrylate (DEGMA), methacrylic acid (MAA), and ethylene glycol dimethacrylate (EGDMA) were dissolved in 48 mL Milli-Q water in a 250 mL three-neck round-bottom flask. After 10 min, hydroxy ethyl methacrylate-coupled azobenzene (HEMA-Az) dissolved in

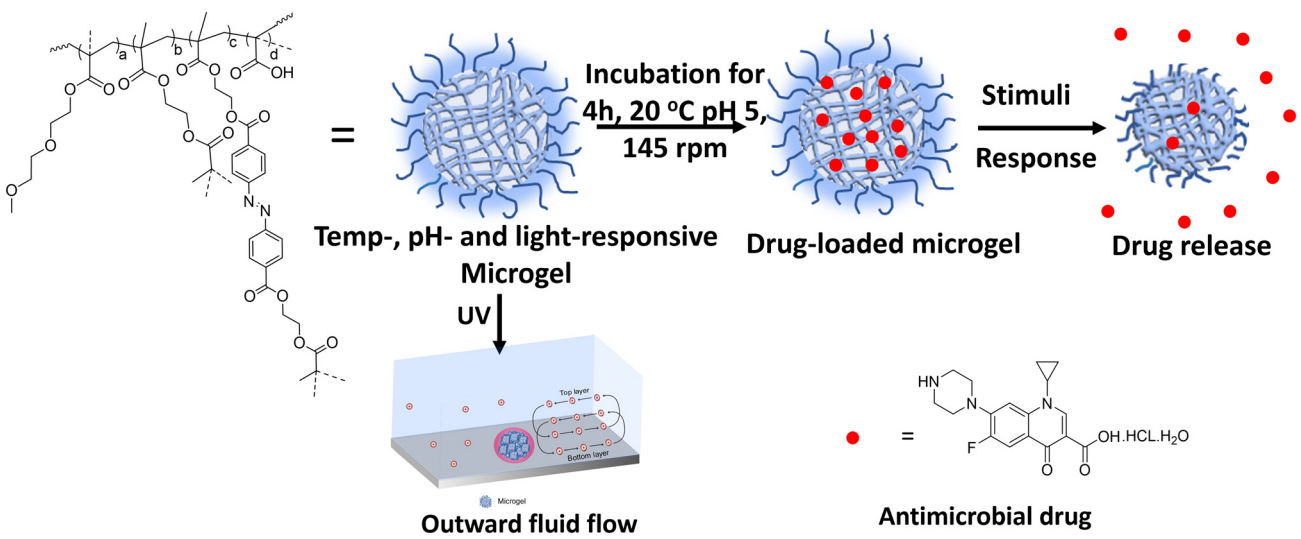

Scheme 1 Schematic of drug loading and release from the multi-responsive microgel in the presence of stimuli.

Table 1 Composition of the microgels as per the initial monomers

MG	DEGMA (mol%)	MAA (mol%)	EDGMA (mol%)	HEMA-Az (mol%)
M0	88	10	2	0
M1	88	10	1.5	0.5
M2	88	10	1	1

1 mL ethanol was added to the reaction mixture (*cf.* ESI, Fig. S1 and 2†). The reaction mixture was heated to 70 °C under an inert atmosphere. After 1 h, an initiator (KPS) dissolved in 1 mL was added to initiate polymerization. The reaction was allowed to proceed for 6 h. After completion of the reaction, the sample was then centrifuged at 10 000 rpm for 40 min followed by two repeated washings for purification. Finally, the samples were re-dispersed in Milli-Q water and lyophilized for storage (Scheme 2).

UV-visible spectroscopy

The UV-visible spectra were recorded using an Agilent Cary-60 spectrophotometer in the wavelength range of 800 to 200 nm. Irradiation was carried out using 365 nm and 455 nm lasers and was performed inside a UV cuvette with a 10 mm path length. For the irradiation experiments, 10 μL of microgel was diluted to 1 mL using 10% DMSO in water. Further, the irradiation experiments were performed using the lasers until saturation was attained.

Irradiation system

The irradiation assembly was procured from Holmarc Opto-Mechatronics Ltd, Kerala, India with a power input of 230 V/50 Hz. The irradiation set-up included a detector attached with a 365 nm UV laser, which was utilized to irradiate the drug-absorbed microgel samples. The percentage drug release without irradiation was studied using UV spectroscopy after incubating in a vertical oscillation lab incubator at 145 rpm. The percentage drug release from the drug-loaded microgel was estimated under 365 nm UV light irradiation for certain time intervals at different pH.

Dynamic light scattering (DLS)

The phase-transition behaviour of the prepared microgels as a function of temperature, pH, and light was extensively investigated using a Malvern Zetasizer Nano-S90 instrument, wherein the intensity, volume, and number size-distribution data were collected. For the DLS measurements, diluted microgel dispersions with a final concentration of 0.05 wt% were used. The thermoresponsive behaviour was tested within the temperature range of 20–50 °C, allowing a 10 min equilibration time prior to the measurement at each temperature. The pH-responsive behaviour was tested from pH 3 to pH 12. The pH of the samples was adjusted by the addition of acid or base. The microgel samples were irradiated by 365 nm or 465 nm light before the measurement to investigate their light-responsive behaviour. The data presented here are averages from 20 runs with a 10 s acquisition time. The temperature-induced deswelling ratio was calculated by the equation given below:

$$\alpha = \left(\frac{R_h^{20\,°C}}{R_h^{50\,°C}}\right)^3 \quad (1)$$

High-resolution transmission electron microscopy (HR-TEM)

TEM images were recorded using a JEOL JEM 2100 microscope with a tungsten filament at an accelerating voltage of 200 kV. For the sample preparation, a 0.05 wt% aliquot of aqueous microgel dispersion was drop-cast on a 200-mesh carbon-coated Cu grid. The samples were further vacuum-dried overnight prior to loading them in the instrument. The obtained TEM images were then analysed with ImageJ software.

Fluid-flow study

A thin layer of PDMS sheet with a small circular aperture in the centre (d = 4.6 mm) was first made and placed on the glass slide in such a manner that the circular opening remained in

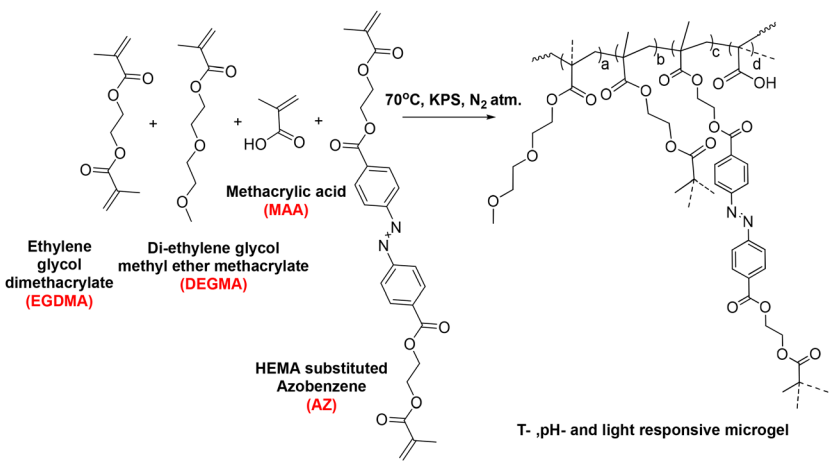

Scheme 2 Schematic of the synthesis of the azobenzene-based multifunctional microgels.

the middle of the slide. Then, the glass slide was dipped in 1 wt% PEI solution to selectively activate the patch. Subsequently, the microgel dispersion was drop-cast onto the activated patch and allowed to dry overnight. The microgel was thus immobilized on the glass slide through H-bonding and electrostatic interactions. Later, the PDMS film was peeled off to leave the microgel pattern on the glass slide. Next, a customized chamber with the dimensions of length = 1 cm, width = 1 cm, height = 1.8 mm was placed on the glass slide and sealed with a PET sheet. An aqueous solution containing tracer particles (5 μm in diameter) was introduced into the chamber to initiate fluid pumping. An Olympus IX73 inverted optical microscope with a 100 W halogen lamp was used to observe the fluid flow. The sample in the chamber was irradiated with laser light at wavelengths of 365 nm and 455 nm to investigate the light-responsive fluid-flow behaviour. Real-time footage depicting the motion of the particles was recorded for subsequent analysis. To assess the velocity of the fluid, a total of 10 particles were monitored over 30 s using Tracker software (motion analysis software).

Drug loading

Ciprofloxacin (**Cf**), an antimicrobial drug, was loaded into the microgel (**M2**) and its calibration curve was plotted at 272 nm. Specifically, **Cf** was loaded into the crosslinked microgel to obtain a dispersion of 4 wt%, 1 mL. The dispersion (pH 5) was then mixed with aqueous ciprofloxacin (1 mg mL^{-1}, 500 μL). Further, it was stirred vigorously in a vertical oscillation lab incubator at 145 rpm for 4 h at 25 °C. The **Cf**-loaded crosslinked microgel was then centrifuged to remove any free drug. The drug-loading content was analysed by UV-visible spectroscopy at 272 nm based on a calibration curve obtained with varied drug concentrations. The drug-loading content (DLC) and drug-loading efficiency (DLE) were calculated[51,52] using the following equations:

$$\text{Drug-loading content} = \frac{\text{wt of drug in microgel}}{\text{wt of microgel}} \times 100 \quad (2)$$

$$\text{Drug-loading efficiency} = \frac{\text{wt of drug in microgel}}{\text{wt of feeding drug}} \times 100 \quad (3)$$

Drug release

The drug-release behaviour of the microgel was investigated at pH 7.4, 9, and 5.4 with and without 365 nm UV-light irradiation. For the release of **Cf** from the microgel in the crosslinked state, the **Cf**-loaded microgel (4 wt%) was dispersed in phosphate-buffered saline (PBS) of pH 7.4. The dispersion was centrifuged (7000 rpm for 30 min) and the supernatant solution (1 mL) was analysed by UV-visible spectroscopy at 272 nm to determine the amount of **Cf** released. The sample condition was maintained at 37 °C or 25 °C using a magnetic stirrer. The **Cf**-loaded microgel was subsequently re-dispersed into the supernatant solution for further release testing at time intervals of 0.5, 1, 2, 3, 4, 5, 6, 9, and 19 h. For assessing photoresponsive **Cf** release, the microgel was irradiated at 365 nm during incubation.

Results and discussion

Design and characterization of the microgels

Microgels were prepared using a free radical precipitation polymerization method with the monomers DEGMA, MAA, and crosslinkers EGDMA and HEMA-Az (Scheme 2). Incorporation of the azobenzene-tethered crosslinker was expected to make the microgels photoresponsive. The overall mol% of the crosslinkers was maintained constant at 2%, whereas the concentration of the individual crosslinkers was tuned, as given in Table 1. Thus, the **M0** microgel with EGDMA as the crosslinker only was considered as the control microgel. For the syntheses of microgels **M1** and **M2**, 0.5 mol% and 1 mol% of HEMA-Az were used as the photoresponsive crosslinker alongside EGDMA to keep the overall crosslinking density intact. The morphological features of the prepared microgels were characterized by TEM, which revealed the spherical morphology of the **M0** and **M1** microgels with a core–corona structure (Fig. 1A and B). Notably, the core was dense with a fuzzy corona, owing to the fluctuations in density within the microgel network, which led to the particles developing an outer edge that was slightly uneven. However, the core–corona morphology was not distinctly observed in the **M2** microgel owing to its denser core structure (Fig. 1C). This could be presumably attributed to the increase in hydrophobic density in the microgel network, which promoted increased hydrophobic interaction in the constrained core in the **M2** microgel. The average diameters of **M0**, **M1**, and **M2** were 395.7 ± 33, 290 ± 37, and 253 ± 34 nm, as determined from the TEM images, respectively (Fig. S3†). DLS data obtained as intensity, number, and volume percentages showed narrow size distributions for the microgels at the elevated temperature of 60 °C (Fig. 1D and S4†). The DLS data corroborated well with the sizes obtained from the TEM analysis with the slight hydrodynamic diameters (Fig. 1E). Notably, the size of the microgel particles was reduced with the increase in azobenzene content. The formation of smaller particles with the presence of a high content of azobenzene in the microgels could be attributed to the increase in hydrophobicity and the comparatively high degree of crosslinking in the presence of the azobenzene-based crosslinker. Next, we monitored the surface charges of the microgels at different pH by zeta potential measurement (Fig. 1F). The microgels were found to be negatively charged with almost similar values (~−8 mV) owing to the deprotonation of the methacrylic acid. Interestingly, the accumulation of negative surface charge increased (~−18 mV) upon increasing the pH from 5 to 9.

Stimuli-responsiveness of the microgels

Next, we investigated the stimuli-responsive behaviour of the microgels towards external conditions, such as temperature, pH, and light. DLS data recorded as a function of temperature

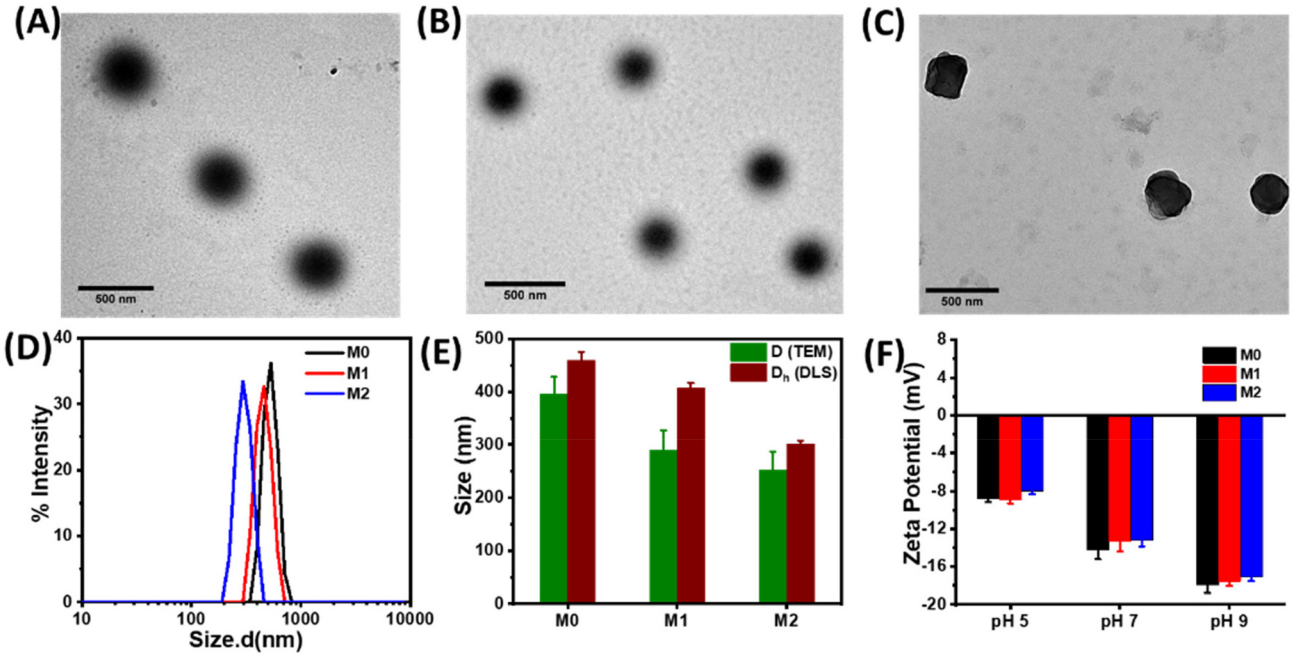

Fig. 1 TEM images of the microgels (A) **M0**, (B) **M1**, and (C) **M2** drop-cast at 50 °C. (D) DLS data for the percentage intensity distribution of the microgels at 60 °C and (E) comparison of the sizes obtained from the TEM and DLS data. (F) Zeta potential of the microgels at different pHs. Sample concentration = 0.5 mg mL^{-1}. TEM and DLS data were recorded at pH 7.

furnished the hydrodynamic diameter (D_h) as a result of the temperature-induced phase-transition behaviour of the microgels (Fig. 2A–C and S5†). The pH of the microgels was maintained at pH 7. At 20 °C, the aqueous dispersions of all the microgels exhibited much higher hydrodynamic diameters, corresponding to the swollen states, while at higher temperatures, the typical volume phase transition from the swollen to collapsed state led to a decrease in the D_h values of the microgels. This could be attributed to the breaking of the hydrogen bonding between the microgels and water molecules at elev-

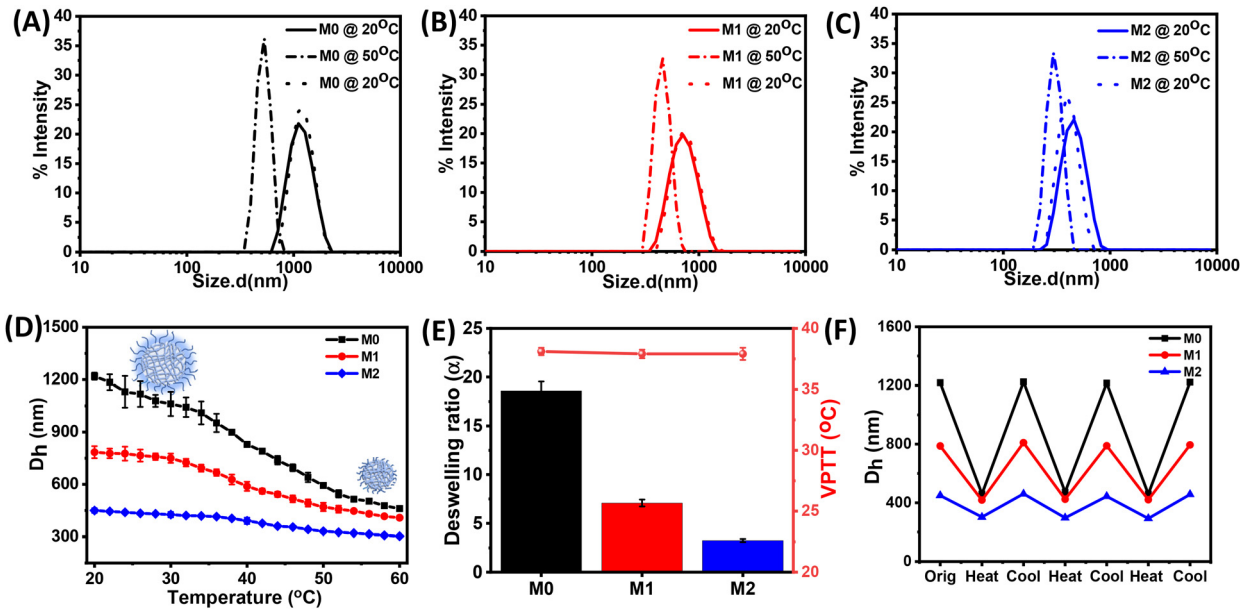

Fig. 2 (A–C) DLS data for the temperature-induced reversible swelling/deswelling of **M0**, **M1**, and **M2** microgels, respectively. (D) Variation in the hydrodynamic diameter (D_h) of the microgels with a gradual increase in temperature, showing their swollen and collapsed states. (E) Temperature-induced deswelling ratios and VPTTs for the microgels at 60 °C. (F) DLS data showing the reversibility of the temperature-induced swelling/deswelling for up to 3 cycles. Sample concentration = 0.5 mg mL^{-1}, pH 7.

ated temperatures. Such temperature-induced phase transition was found to be reversible upon decreasing the temperature. The size of the microgel particles gradually reduced with the increase in the temperature in the range from 20 °C to 60 °C (Fig. 2D). It was noteworthy that the azobenzene-based microgels (**M1** and **M2**) showed less thermosresponsiveness compared to the control microgel (**M0**). This was presumably due to the fact that the azobenzene crosslinker increased the hydrophobic content in the microgel network to ultimately reduce the swelling capacity of the particles.[53,54] The obtained deswelling ratios of the microgels clearly revealed that the swelling capacity of the microgels was significantly reduced from **M0** to **M2** from 18.6 to 3.3 (Fig. 2E). However, there was no significant change observed in the volume phase-transition temperature (VPTT) of the microgel particles, which were found be ~38.1 °C, ~37.9 °C, and ~37.9 °C for **M0**, **M1**, and **M2**, respectively. Interestingly, all the microgels exhibited a reversible thermoresponsive behaviour with respect to the size, *albeit* to different extents, when subjected to an alternating cycle of heat–cool annealing between 20 °C and 60 °C (Fig. 2F).

Furthermore, we investigated the pH-induced phase-transition behaviour of the microgels at different pHs (Fig. 3A–C). We observed narrow size-distribution profiles for the microgels and a significant increase in the hydrodynamic diameter (D_h) upon increasing the pH to 12 at 25 °C from the detailed analysis of the DLS intensity, volume, and number data (Fig. S6†). Interestingly, such a pH-driven increase in D_h was reversible upon reverting the pH to 4. Here, at high pH, the carboxylic (–COOH) groups of MAA in the microgel particles underwent deprotonation to form carboxylate ions ($–COO^-$) (pK_a of MAA ~4.7) and exhibited considerable electrostatic repulsion. This resulted in further water intake inside the microgel network, *i.e.* more swelling of the microgels.[55,56] Furthermore, the change in D_h of the microgels was investigated by DLS upon the gradual increase in the pH from 3 to 12 (Fig. 3D). The pH-driven swelling ratios of the microgels clearly revealed there was no specific trend (Fig. 3E), as the extent of the MAA was constant. This corroborated with the fact that the protonation/deprotonation of MAA controlled the pH sensitivity of the microgels. AFM images for **M2** corroborated their height as ~15 ± 2 nm at pH 12 compared to their height as ~6 ± 1 nm at pH 4 (Fig. 3F and G).

The incorporation of the azobenzene crosslinker prompted us to study the photoresponsiveness of the microgel particles. Interestingly, the HEMA-Az molecule exhibited excellent reversible *trans* to *cis* isomerization of azobenzene upon irradiation with the 365 nm light for 10 min (Fig. S7†). The absorbance at 335 nm decreased while another peak at 430 nm appears, which was attributed to π–π* and n–π* transitions, respectively. We were curious to explore the implication of such photoswitching of the HEMA-Az crosslinker in the spatially constrained environment of the microgel network. Notably, the azobenzene-incorporated microgels also exhibited a photoisomerization behaviour, *albeit* with a rather longer irradiation time, as monitored from the UV-vis spectra. Thus, upon irradiation with UV light (365 nm), **M2** exhibited a gradual reduction of the characteristics at 335 nm and an increase in the 430 nm peak over 20 min, indicating *trans* to *cis* isomerization, which could be retrieved within a minute upon shinning visible light (455 nm) on the sample (Fig. 4A–C). On the contrary, the **M1** microgel showed faster *trans* to *cis* photoisomerization kinetics owing to its lower incorporation of the hydro-

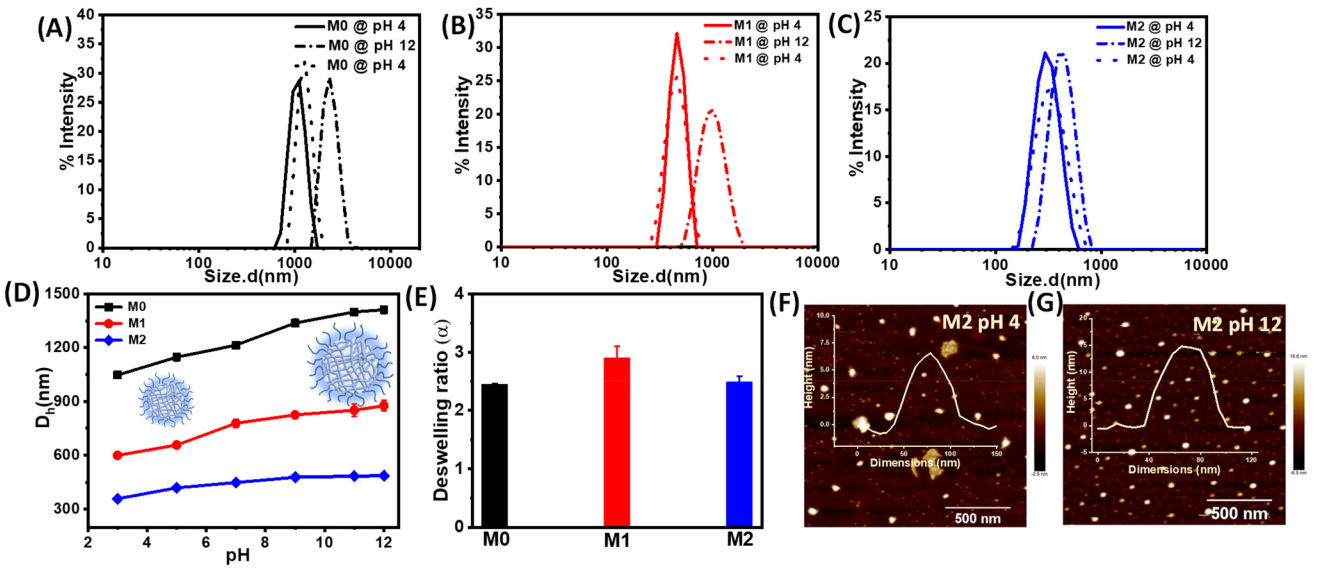

Fig. 3 (A–C) DLS intensity data showing pH-induced reversible swelling/deswelling of the microgels **M0**, **M1**, and **M2**. (D) Variation in the hydrodynamic diameter (D_h) of the microgels as a function of pH, showing their swollen and collapsed states. Sample concentration = 0.5 mg mL^{-1}, T = 25 °C. (E) Histogram showing the pH-induced de/swelling factors for the microgels. (F–G) AFM height images of the **M2** microgels at pH 4 and 12, respectively.

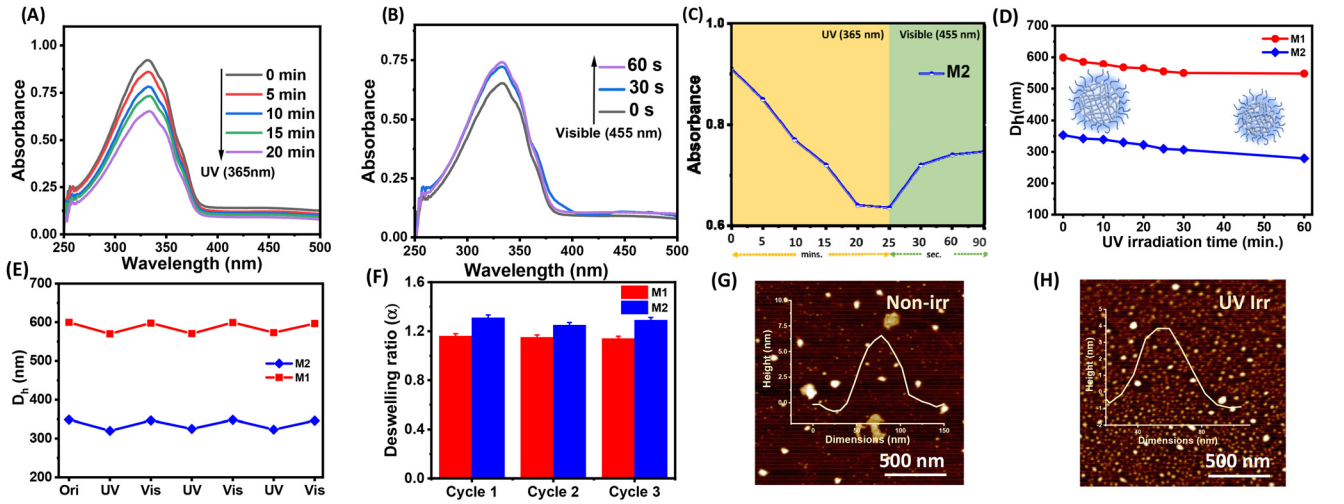

Fig. 4 Photoswitching behaviour of **M2** microgel. (A) *trans* to *cis* photoconversion upon irradiation with UV light (365 nm) for 20 min and (B) *cis* to *trans* photoconversion upon irradiation with visible light (455 nm) for 1 min. (C) Reversible photoisomerization of **M2** microgel by consecutive irradiation using UV (365 nm) and visible (455 nm) light. (D) Change in the hydrodynamic diameter with increasing the UV irradiation time, showing the transition between the swollen and collapsed microgels. (E) Reversibility of the photoswitchable swelling/deswelling for **M1** and **M2** microgels and (F) the deswelling ratios of **M1** and **M2** over three cycles. (G and H) AFM height images for **M2** microgel before and after UV irradiation. Sample concentrations = 0.5 mg mL^{-1}, T = 30 °C, pH 5.

phobic azobenzene crosslinker, which made the microgel core less compact (Fig. S8†). Such slower *trans* to *cis* photoisomerization kinetics for **M2** indicated a greater activation energy barrier, owing to the constraint environment present in the dense hydrophobic core of the microgel network. Next, we performed DLS analysis to investigate the implication of such reversible photoswitching over the swelling/deswelling behaviour of the microgels. Fig. 4D shows the gradual reduction in D_h for both **M1** and **M2** with increasing the irradiation time. This accorded with the findings of Phua *et al.*,[57] who reported that their microgels underwent rapid deswelling even though the *trans* isomers were converted into the more polar *cis* isomers. The constricted spatial arrangement of the azobenzene motif embedded in the microgel as a crosslinker played a significant role in such deswelling. Also, the *cis* state has a higher free-volume requirement than the *trans* state, and to accommodate the *cis* form in the microgel network, water molecules are excluded by breaking the hydrogen bonds. The exclusion of water results in entropic gain while breaking the hydrogen bonding raises the enthalpy, *i.e.* entropic and enthalpic compensation is required to accommodate the *cis* form.[58] Further, upon irradiation of visible light the microgel particles reswelled, and such the reversibility of photoinduced swelling/deswelling was demonstrated for up to 3 consecutive cycles (Fig. 4E). Interestingly, the deswelling factor of **M2** (~1.31) was found to be slightly better than that of **M1** (~1.14) over the three cycles (Fig. 4F). This might be due to the higher concentration of the azobenzene crosslinker present in **M2**. Expectedly, the control microgel **M0** did not show any swelling/deswelling in response to photoirradiation. The AFM height images showed a contraction of the height for the microgel **M2** from ~6 ± 1 nm to ~4 ± 1 nm upon UV irradiation (Fig. 4G and H).

Actuating microgel with fluid-flow control

The photoresponsive swelling/deswelling of the microgels prompted us to explore their potential for micropump actuation by fluid movement, with an aim for extraordinary precision at the microscale level. Consequently, we conducted an investigation wherein **M1** and **M2** microgels (pH 5) were immobilized within micropump chambers in a circular pattern (4.6 mm diameter) through hydrogen bonding and electrostatic interactions (Fig. 5A). Our experimental set-up involved injecting an aqueous solution containing suspended tracer particles (5 μm in diameter) into the chamber. Initially, we observed an inward flow, *i.e.* fluid moved towards the film in the case of the **M2** microgel at a velocity of 0.66 ± 0.0941 μm s^{-1} due to the hydrophilicity of the microgel (Fig. 5B). However, after approximately 4 to 5 min the fluid flow ceased as the microgels reached equilibrium with the surroundings. Upon UV-light irradiation, a reversal in the fluid flow direction was observed, with the fluid moving outward, *i.e.* away from the film, at a velocity of 1.35 ± 0.0834 μm s^{-1} (*cf.* ESI, Movie SV1†). This outward flow phenomenon was attributed to the response of the azobenzene molecules within the microgel to UV irradiation. Upon exposure, the *trans* isomer of azobenzene undergoes a transformation into the *cis* state. Remarkably, the *cis* state demands a larger free volume compared to the *trans* state, compelling the microgel network to exclude water molecules. This exclusion mechanism is facilitated by the disruption of hydrogen bonds, consequently driving the fluid to flow outward from the microgel film.

Moreover, when exposed to visible light, an intriguing reversal occurred, with the fluid now flowing towards the microgel film with a velocity of 2.35 ± 0.0794 μm s^{-1} (*cf.* ESI, Movie

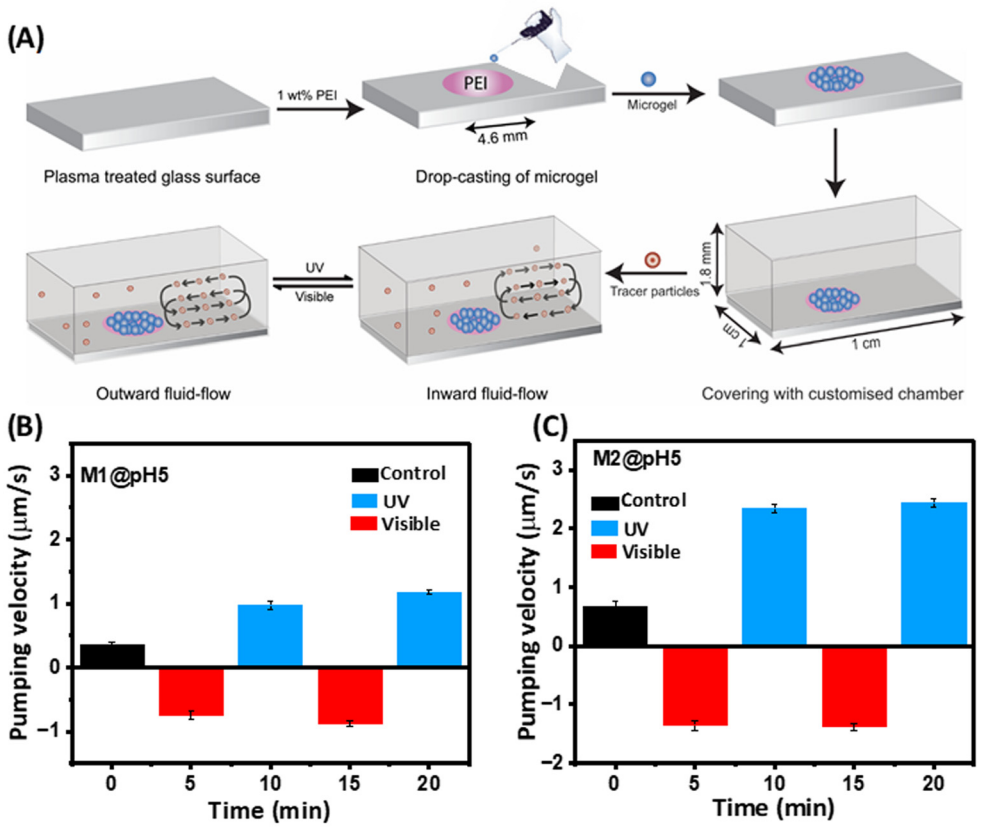

Fig. 5 (A) Schematic representation of the fabrication of a fluid-flow pump and the light-induced reversal of the fluid-flow direction. (B) Pumping velocity of **M2** microgel at pH 5. (C) Pumping velocity of **M1** microgel at pH 5. Here, the positive and negative velocity represent the inward and outward fluid-flow, respectively.

SV2†). This oscillatory behaviour of the fluid indicated a dynamic response to light stimuli. Such fluid-flow reversal was based on the reversible nature of the azobenzene molecule's photoisomerization. Under visible light, the *cis* state showed a transition back to the *trans* state, reducing the free volume requirement and allowing the microgel to reabsorb water molecules, thus drawing fluid towards the film. A fluid-flow pattern akin to **M2** was observed with the **M1** microgel, but with a slower velocity, attributed to the lower concentration of azobenzene present within the **M1** microgel structure (Fig. 5C). Notably, these studies were also done at pH 7, but no directional flow was observed. Further, we estimated the stability of the microgel **M2** after immersion in different culture media, *e.g.* PBS, FBS, DMEM, and HF12. The zeta potential data of **M2** monitored over 7 days did not show any observable difference, indicating the microgel was stable (Fig. S9A†). To further evaluate the cytotoxicity of the microgels, we performed an MTT assay with the L929 mice fibroblast cell line, which revealed a greater than 80% biocompatibility of **M2** over a broad concentration range (Fig. S9B†).

Drug-loading studies

Following the successful demonstration of the photoresponsive microgels effectiveness in the actuation pump study, we speculated that they might be able to modulate the fluid flow with subsequent diffusion and mass transfer. Thus, we aimed to exploit such photoactuation of the microgels for stimuli-responsive drug delivery. Since the **M2** microgel showed a better fluid flow and photoactuation behaviour, we selected this system for the on-demand stimuli-responsive release studies. Ciprofloxacin (**Cf**), an antibiotic drug used in microbial infections, was chosen for the drug-loading and -release study. Interestingly, the drug (**Cf**) has two pK_a at pH 6.1 and 8.8 owing to the presence of carboxylic acid and amine motifs, respectively. Thus, the zeta potential values of **Cf** at pH 5, 7, 9 were found to be ~0.19, ~−6.89, and −12.32 mV, respectively (Fig. 6A). This indicated that at pH 5, the drug remained in a cationic form while at pH 7 and higher the drug became negatively charged. The zeta potential of the **M2** microgel showed an increase in negative charge with increasing the pH, owing to the presence of MAA having a pK_a of 4.7.

With consideration of the zeta potential values of **Cf** and the microgels, the drug-loading studies were performed at 25 °C at different pHs. The changes were monitored by UV-vis spectroscopy to ensure the maximum **Cf** absorption by the microgel network *via* physical diffusion, hydrophobic interactions, and electrostatic interactions. The drug-loaded microgels showed negative zeta potentials at all the pHs.

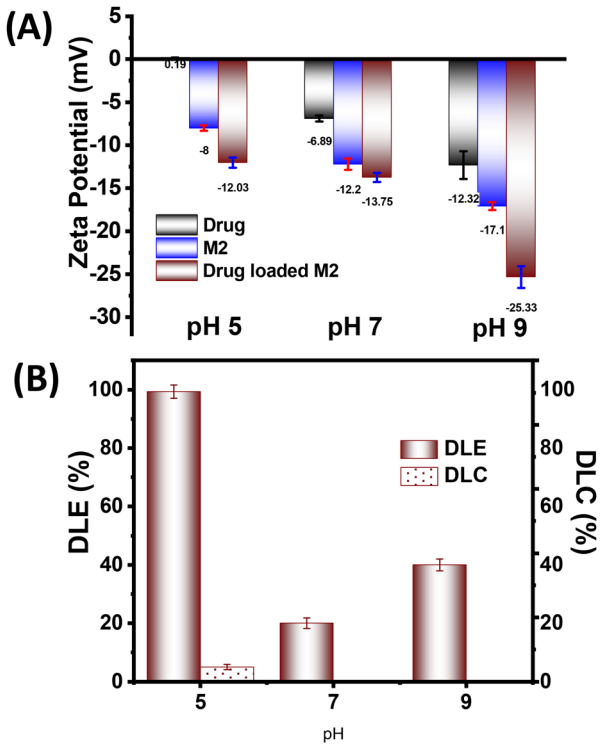

Fig. 6 (A) Zeta potential of ciprofloxacin showing the drug in a cationic form (positively charged) at acidic pH and in anionic form (negatively charged) at basic pH along with **M2** and the drug-loaded **M2** microgel. (B) Drug-loading content and efficiency at different pHs.

Interestingly, at pH 5 the drug-loading content (DLC) and drug-loading efficiency (DLE) were found to be the best, with values of 4.97% and 99.4%, respectively (Fig. 6B). This was presumably due to the enhanced electrostatic interaction of the cationic form of the drug with the negatively charged microgel. Moreover, the swelling of the microgels at higher pH led to higher diffusion, besides the electrostatic repulsion, which rendered a lower drug loading.[59] Thus, we observed a DLC of 0.11% and DLE of 20% at pH 7, while at pH 9, they were found to be 0.23% and 40%, respectively. Thus, we optimized the drug-loaded **M2** microgel at pH 5 for the further drug-release studies.

Stimuli-responsive drug release

Next, we performed drug-release experiments by subjecting the **Cf**-loaded **M2** microgel to different stimuli of pH, temperature, and light. The microgel was placed in phosphate buffer media of pH 5.4, 7.4, and 9 maintained at a temperature of 25 °C and 37 °C. The media with pH 5.4, 7.4 and 9 mimic the endolysosomal compartment, extracellular pH, and wound environment, respectively. Notably, the temperatures (25 °C and 37 °C) were below and above the VPTT of the microgel; therefore, enabling a possible understanding of the drug-release pattern with respect to pH and temperature. Moreover, the photoswitching behaviour of the microgels mediated by the photoisomerization of azobenzene was also probed towards

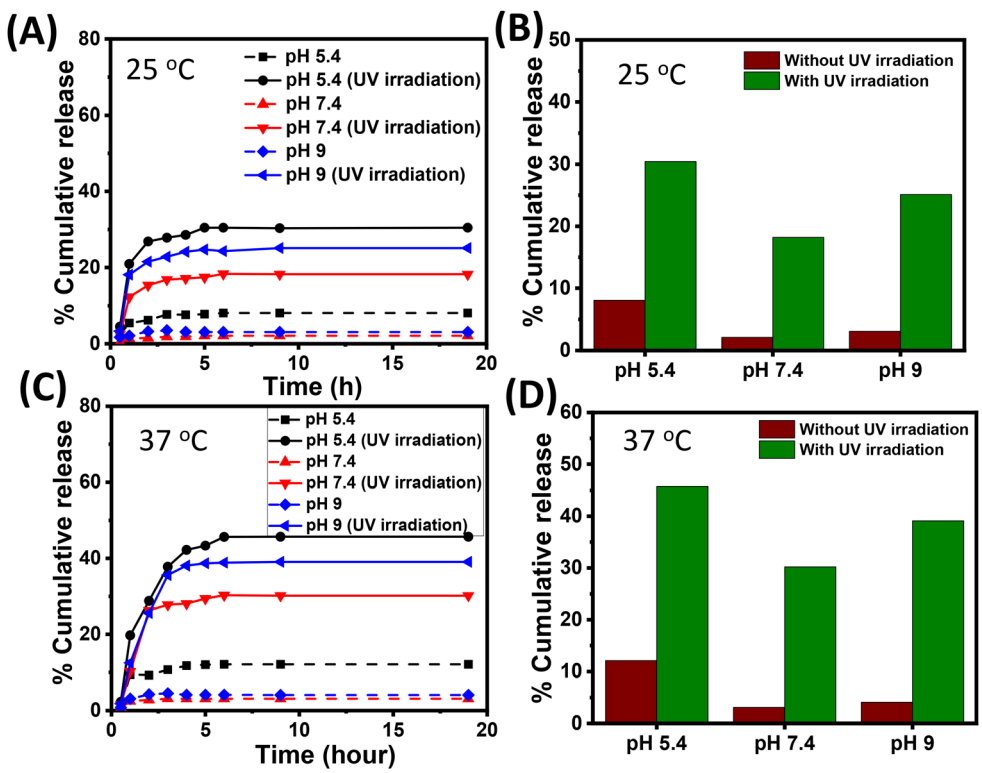

Fig. 7 Stimuli-responsive drug release profile with time and corresponding histogram of the cumulative release of ciprofloxacin-loaded **M2** microgels in different external pH media without and with photostimulus at (A and B) 25 °C and (C and D) 37 °C. UV irradiation at 365 nm.

obtaining the photoresponsive drug-release pattern, inspired from the actuating fluid-flow pump model.

Henceforth, 12 simultaneous delivery conditions were selected without irradiation and with irradiation (λ = 365 nm) at two temperatures (25 °C and 37 °C) along with three pH conditions (5.4, 7.4, and 9) in order to control the release of **Cf** from the microgel (*cf.* ESI, Fig. S10†). Fig. 7A and B give the release data of **M2** microgel placed in phosphate media of pH 5.4, 7.4, and 9 maintained at 25 °C without and with light irradiation. At pH 7.4 and pH 9, we observed a negligible amount of drug release (~2% and ~3%, respectively) over 20 h. However, at pH 5.4 the loaded **M2** microgel demonstrated a slightly higher (~8%) percentage of drug release. This was presumably due to lowering the electrostatic interaction of the microgel at pH 5.4 and the drug, leading to the passive diffusion of **Cf** from the hydrophobic core of the microgel. Interestingly, upon UV irradiation, the **M2** microgel at pH 5.4 exhibited ~30% cumulative drug release, while cumulative drug release was noted to be ~18% and ~25% at pH 7.4 and 9, respectively. It is noteworthy that minimal electrostatic attraction existed between the positively charged ammonium ion of **Cf** and the microgel due to the increased protonation of the $-COO^-$ groups. Thus, the light-mediated photoisomerization of azobenzene directly impacted the hydrophobic core of the microgels to prompt **Cf** release. Such differences in the drug-release extent at higher pH might account for the extent of the photoswitching at those pHs. This corroborated the fluid pump actuation study, where the flow velocity was found to be highest at pH 5. Moreover, differential repulsive electrostatic interactions between the negatively charged drug and microgels might play a role in the comparatively higher release at pH 9.

Next, we performed drug-release experiments at the physiological temperature of 37 °C, which was above the VPTT of the **M2** microgel. This incidentally paved the way for the temperature-mediated volume phase transition of the drug-loaded microgels to greatly enhance the **Cf** release at 37 °C. Fig. 7C and D show the release data for **M2** microgel placed in phosphate media of pH 5.4, 7.4, and 9 maintained at 37 °C in the dark and under light irradiation. We noted the drug-release pattern attained a plateau within 20 h, where, **Cf** release from the microgels showed an initial burst effect within 2 h, owing to the enhanced diffusion process from the microgel interior, and later maintained a sustained effect for up to 19 h. This could be an outcome of the hydrophobic azobenzene inner core concomitantly reducing the diffusion mechanism.[18,60] This alternate release profile could probably ascribe to the temperature along with the pH sensitivity of the loaded microgels along with change in hydrophilicity of the drug in accordance with the pH and light. In the dark condition at pH 5.4, a cumulative release of 12% of **Cf** was observed, while at pH 7.4 and pH 9, a negligible amount (~3% and ~4%, respectively) of drug release was noted. This could presumably be attributed to the passive release of **Cf** and the temperature-mediated collapse of the hydrophobic core in comparison to the case at 25 °C. However, upon light irradiation at acidic pH 5.4, the maximum cumulative drug release was noted to be approximately 45%, whereas at pH 7.4 and 9, it was 30% and 39%, respectively. Here, the **M2** microgel system was in a collapsed state because of MAA and the more profound light interaction with the core at pH 5.4. The combination of increased temperature and light irradiation upon the **M2** microgel and the increased drug solubility under acidic condition contributed to the improved drug release.[32]

The drug-release kinetics were fitted with different pharmacokinetic models, including zero, first, Higuchi, and Korsmeyer–Peppas model, in order to analyze the release pattern of the microgel systems under different conditions (Fig. S11, 12 and Table S1†). For the Korsmeyer–Peppas model, better R^2 values were found showing it to be most suitable fitting model. The diffusion exponent (n) of less than 0.5 indicated it followed a Fick's law of diffusion mechanism. Interestingly, the UV-irradiation-rendered n value between 0.5–1 t suggested a combination of diffusion and erosion to be the ideal mechanism of drug release. Furthermore, drug release at lower pH exhibited higher k_{KP} values, indicating the pH-mediated shrinking mechanism of the microgel enhanced the drug-release rate. Notably, the optimized size of the microgel ensured a significant barrier to entering the bloodstream through damaged endothelial cells. We anticipate that these microgels would predominantly remain localized while ensuring effective and sustained drug release at a wound site.

Conclusions

To summarize, we designed multi-responsive (temperature-, pH-, and light-responsive) microgels with the different contents of azobenzene crosslinkers, denoted as **M0**, **M1**, **M2**. The effective incorporation of the azobenzene-based polymer into the microgel network furnished the microgels network with the distinctive photoisomerization property of azobenzene. Furthermore, the microgels exhibited reversible swelling/deswelling behaviour with temperature, pH, and light stimuli. Notably, the size and deswelling ratio of the microgels were reduced with the increase in azobenzene content owing to the increased overall hydrophobicity of the microgels. Furthermore, the **M2** microgel system exhibited excellent photoactuation, which was exploited for controlling the fluid-flow pattern *via* inward and outward flow for the first time. Such modulation of the fluid flow with subsequent diffusion and mass transfer propelled by photoactuation of the microgel was explored in stimuli-responsive drug (**Cf**) release experiments. The drug was loaded in **M2** microgel at 25 °C and pH 5, with an excellent adsorption capacity of 49.7 μg per milligram. *In vitro*-release experiments were performed by adjusting the temperature, pH, and light conditions, exhibiting ~45% on-demand release in the presence of UV light at 37 °C and pH 5.4. Such an azobenzene-based microgel system was demonstrated to be a promising option for light-responsive topical delivery. In this study, we highlighted azobenzene-based multifunctional microgels and their capability to achieve on-demand drug release in response to various

stimuli. Such stimuli-responsive microgels with tailored biochemical, mechanical, and structural characteristics might also find application in catalysis, enzyme immobilization, and tissue engineering. This feature has the potential to accelerate the development of functional systems intended for biomedical applications, and work towards that direction is already underway in our laboratory.

Data availability

The data supporting this article have been included as part of the ESI.†

Conflicts of interest

There are no conflicts to declare.

Acknowledgements

The authors are thankful to Institute of Nano Science and Technology (INST), Mohali for providing infrastructure and characterization facilities. PA expresses gratitude for financial support from NPDF grants (PDF/2022/002652) and DD thanks SERB-TARE grant (TAR/2022/000526).

References

1 V. Maffeis, L. Heuberger, A. Nikoletić, C. Schoenenberger and C. G. Palivan, *Adv. Sci.*, 2024, **11**, 2305837.
2 H. Lu, A. Blokhuis, R. Turk-MacLeod, J. Karuppusamy, A. Franconi, G. Woronoff, C. Jeancolas, A. Abrishamkar, E. Loire, F. Ferrage, P. Pelupessy, L. Jullien, E. Szathmary, P. Nghe and A. D. Griffiths, *Nat. Chem.*, 2024, **16**, 70–78.
3 L. J. Rothschild, N. J. H. Averesch, E. A. Strychalski, F. Moser, J. I. Glass, R. Cruz Perez, I. O. Yekinni, B. Rothschild-Mancinelli, G. A. Roberts Kingman, F. Wu, J. Waeterschoot, I. A. Ioannou, M. C. Jewett, A. P. Liu, V. Noireaux, C. Sorenson and K. P. Adamala, *ACS Synth. Biol.*, 2024, **13**, 974–997.
4 B. C. Buddingh and J. C. M. Van Hest, *Acc. Chem. Res.*, 2017, **50**, 769–777.
5 S. Wu, M. Zhu, D. Lu, A. H. Milani, Q. Lian, L. A. Fielding, B. R. Saunders, M. J. Derry, S. P. Armes, D. Adlam and J. A. Hoyland, *Chem. Sci.*, 2019, **10**, 8832–8839.
6 N. T. Nguyen, J. Jennings, A. H. Milani, C. D. S. Martino, L. T. B. Nguyen, S. Wu, M. Z. Mokhtar, J. M. Saunders, J. E. Gautrot, S. P. Armes and B. R. Saunders, *Biomacromolecules*, 2022, **23**, 1423–1432.
7 H. F. Mathews, M. I. Pieper, S. Jung and A. Pich, *Angew. Chem., Int. Ed.*, 2023, **62**, e202304908.
8 M. Abbas, W. P. Lipiński, J. Wang and E. Spruijt, *Chem. Soc. Rev.*, 2021, **50**, 3690–3705.
9 H. Tsurusawa and H. Tanaka, *Nat. Phys.*, 2023, **19**, 1171–1177.
10 F. A. Plamper and W. Richtering, *Acc. Chem. Res.*, 2017, **50**, 131–140.
11 K. K. Nakashima, M. H. I. van Haren, A. A. M. André, I. Robu and E. Spruijt, *Nat. Commun.*, 2021, **12**, 3819.
12 A. Ianeselli, D. Tetiker, J. Stein, A. Kühnlein, C. B. Mast, D. Braun and T.-Y. Dora Tang, *Nat. Chem.*, 2022, **14**, 32–39.
13 Y. Ji and Y. Qiao, *Commun. Chem.*, 2024, **7**, 122.
14 A. A. Gavrilov and I. I. Potemkin, *Soft Matter*, 2018, **14**, 5098–5105.
15 K. Gawlitza, C. Wu, R. Georgieva, D. Wang, M. B. Ansorge-Schumacher and R. V. Klitzing, *Phys. Chem. Chem. Phys.*, 2012, **14**, 9594.
16 A. Dan, P. Agnihotri, M. Brugnoni, E. Siemes, D. Wöll, J. J. Crassous and W. Richtering, *Chem. Commun.*, 2019, **55**, 7255–7258.
17 P. Agnihotri and A. Dan, *ACS Appl. Nano Mater.*, 2022, **5**, 10504–10515.
18 N. Singh, S. Aery, S. Juneja, L. Kumari, M. S. Lone, A. A. Dar, S. V. Pawar, S. K. Mehta and A. Dan, *ACS Appl. Bio Mater.*, 2022, **5**, 3487–3499.
19 T. Kageyama, L. Yan, A. Shimizu, S. Maruo and J. Fukuda, *Biomaterials*, 2019, **212**, 55–63.
20 M.-C. Tatry, P. Galanopoulo, L. Waldmann, V. Schmitt and V. Ravaine, *J. Colloid Interface Sci.*, 2021, **589**, 96–109.
21 P. Agnihotri, Sangeeta, S. Aery and A. Dan, *Soft Matter*, 2021, **17**, 9595–9606.
22 M. Karg, A. Pich, T. Hellweg, T. Hoare, L. A. Lyon, J. J. Crassous, D. Suzuki, R. A. Gumerov, S. Schneider, I. I. Potemkin and W. Richtering, *Langmuir*, 2019, **35**, 6231–6255.
23 N. M. B. Smeets and T. Hoare, *J. Polym. Sci., Part A: Polym. Chem.*, 2013, **51**, 3027–3043.
24 Y. Gao, A. Ahiabu and M. J. Serpe, *ACS Appl. Mater. Interfaces*, 2014, **6**, 13749–13756.
25 K. Zhang and X. Y. Wu, *J. Controlled Release*, 2002, **80**, 169–178.
26 W.-F. Lai, A. S. Susha and A. L. Rogach, *ACS Appl. Mater. Interfaces*, 2016, **8**, 871–880.
27 G. Agarwal and R. Agarwal, *Small*, 2018, **14**, 1801724.
28 A. Saifi, J. P. Joseph, A. P. Singh, A. Pal and K. Kumar, *ACS Omega*, 2021, **6**, 4776–4782.
29 M. K. Pradhan, D. Gupta, K. R. Namdev, Anjali, C. Migalni, A. Pal and A. Srivastava, *Nanoscale*, 2022, **14**, 15079–15090.
30 M. J. Snowden and M. T. Booty, in *Encapsulation and Controlled Release*, Elsevier, 2005, pp. 141–147.
31 *Special Publications*, ed. D. R. Karsa and R. A. Stephenson, Royal Society of Chemistry, Cambridge, 2007, pp. X001–X002.
32 J. Lutz, *J. Polym. Sci., Part A: Polym. Chem.*, 2008, **46**, 3459–3470.
33 D. Lu, M. Zhu, S. Wu, W. Wang, Q. Lian and B. R. Saunders, *Polym. Chem.*, 2019, **10**, 2516–2526.
34 J. P. Joseph, C. Miglani, A. Singh, D. Gupta and A. Pal, *Soft Matter*, 2020, **16**, 2506–2515.

35 C. Miglani, J. P. Joseph, D. Gupta, A. Singh and A. Pal, *RSC Adv.*, 2021, **11**, 39376–39386.
36 J. P. Joseph, C. Miglani, A. Bhatt, D. Ray, A. Singh, D. Gupta, Md. E. Ali, V. K. Aswal and A. Pal, *Polym. Chem.*, 2021, **12**, 1002–1013.
37 A. Singh, J. P. Joseph, D. Gupta, C. Miglani, N. A. Mavlankar and A. Pal, *Nanoscale*, 2021, **13**, 13401–13409.
38 J. Thomas, N. Gupta, J. P. Joseph, V. Chopra, A. Pal and D. Ghosh, *ACS Biomater. Sci. Eng.*, 2021, **7**, 5798–5809.
39 C. Miglani, M. Banoo, D. Nath, J. Ralhan, S. Sil, J. P. Joseph, S. K. Pal, U. Gautam and A. Pal, *Chem. Commun.*, 2023, **59**, 13195–13198.
40 C. Miglani, J. Ralhan, M. Banoo, D. Nath, S. Sil, S. K. Pal, U. K. Gautam and A. Pal, *ACS Polym. Au*, 2024, **4**, 255–265.
41 J. P. Joseph, N. Gupta, C. Miglani, D. Nath, A. Singh, D. Gupta and A. Pal, *Chem. Mater.*, 2022, **34**, 4364–4374.
42 D. Gupta, A. Bhatt, V. Gupta, C. Miglani, J. P. Joseph, J. Ralhan, D. Mandal, M. E. Ali and A. Pal, *Chem. Mater.*, 2022, **34**, 4456–4470.
43 D. Gupta, V. Gupta, D. Nath, C. Miglani, D. Mandal and A. Pal, *ACS Appl. Mater. Interfaces*, 2023, **15**, 25110–25121.
44 D. Patra, H. Zhang, S. Sengupta and A. Sen, *ACS Nano*, 2013, **7**, 7674–7679.
45 R. Varshney, A. K. Gill, M. Alam, C. Agashe and D. Patra, *Lab Chip*, 2021, **21**, 4352–4356.
46 P. Kobauri, F. J. Dekker, W. Szymanski and B. L. Feringa, *Angew. Chem.*, 2023, **135**, e202300681.
47 W. A. Velema, W. Szymanski and B. L. Feringa, *J. Am. Chem. Soc.*, 2014, **136**, 2178–2191.
48 S. H. Lee, B. H. Kim, C. G. Park, C. Lee, B. Y. Lim and Y. B. Choy, *J. Controlled Release*, 2018, **286**, 224–230.
49 J. E. Sayed, C. Lorthior, P. Perrin and N. Sanson, *Soft Matter*, 2019, **15**, 963–972.
50 P. Agnihotri, R. Ritu, K. Dinesh and A. Dan, *Soft Matter*, 2020, **16**, 7845–7859.
51 H. Chopra, S. Bibi, S. Kumar, M. S. Khan, P. Kumar and I. Singh, *Gels*, 2022, **8**, 111.
52 V. Puri, A. Sharma, P. Kumar, I. Singh and K. Huanbutta, *ACS Omega*, 2021, **6**, 15844–15854.
53 L. A. Lyon, Z. Meng, N. Singh, C. D. Sorrell, A. S. John and L. A. Lyon, *Chem. Soc. Rev.*, 2009, **38**, 865–874.
54 B. R. Saunders and B. Vincent, *Adv. Colloid Interface Sci.*, 1999, **80**, 1–25.
55 J. Kleinen, A. Klee and W. Richtering, *Langmuir*, 2010, **26**, 11258–11265.
56 M. Boularas, E. Deniau-Lejeune, V. Alard, J. F. Tranchant, L. Billon and M. Save, *Polym. Chem.*, 2016, **7**, 350–363.
57 D. I. Phua, K. Herman, A. Balaceanu, J. Zakrevski and A. Pich, *Langmuir*, 2016, **32**, 3867–3879.
58 R. H. El Halabieh, O. Mermut and C. J. Barrett, *Pure Appl. Chem.*, 2004, **76**, 1445–1465.
59 A. Pepe, P. Podesva and G. Simone, *Sci. Rep.*, 2017, **7**, 6014.
60 D. Dheer, R. Gupta, D. Singh, A. Magotra, G. Singh, P. N. Gupta and R. Shankar, *ACS Appl. Bio Mater.*, 2019, **2**, 4738–4736.